Strong-Field Kapitza-Dirac Scattering of Neutral Atoms

S. Eilzer,[1] H. Zimmermann,[1] and U. Eichmann[1,2,*]
[1]Max-Born-Institute, 12489 Berlin, Germany
[2]Institut für Optik und Atomare Physik, Technische Universität Berlin, 10623 Berlin, Germany
(Received 29 August 2013; published 17 March 2014)

Laser induced strong-field phenomena in atoms and molecules on the femtosecond (fs) time scale have been almost exclusively investigated with traveling wave fields. In almost all cases, approximation of the strong electromagnetic field by an electric field purely oscillating in time suffices to describe experimental observations. Spatially dependent electromagnetic fields, as they occur in a standing light wave, allow for strong energy and momentum transfer and are expected to extend strong-field dynamics profoundly. Here we report a strong-field version of the Kapitza-Dirac effect for neutral atoms where we scatter neutral He atoms in an intense short pulse standing light wave with fs duration and intensities well in the strong-field tunneling regime. We observe substantial longitudinal momentum transfer concomitant with an unprecedented atomic photon scattering rate greater than $10^{16}\mathrm{s}^{-1}$.

DOI: 10.1103/PhysRevLett.112.113001 PACS numbers: 32.80.Rm, 42.50.Hz

Strong-field phenomena in atoms and molecules induced by an intense traveling wave laser field are successfully described within the dipole approximation taking into account only the time dependency of the electric field, $\vec{E}(\vec{r},t)=\vec{E}(t)$, [1,2]. The magnetic field and spatial field dependencies can usually be neglected due to the weak effective Lorentz force and weak field gradients in the focused laser beam. To fully explore atomic processes in intense electromagnetic fields one might extend the investigations toward spatially dependent strong electromagnetic fields as they occur, e.g., in a standing light wave. This situation, in turn, is intimately connected to the Kapitza-Dirac (KD) effect. The KD effect was originally formulated for the reflection of electrons in a standing light wave [3] and later also extended to neutral atoms [4]. Remarkably, the KD effect in weak standing light waves has been extensively explored in the context of atom optics and manipulation of quantum gases, both theoretically and experimentally [5–8]. The scattering of electrons in strong standing light waves including the relativistic regime, however, has been mainly tackled theoretically, [9–15], in striking contrast to very few experimental studies [16–18]. Two seminal experiments, using very moderate laser intensities $\lesssim 10^{13}$ Wcm^{-2} and pulse durations on the order of hundreds of picoseconds, have been reported on Bragg scattering of free electrons [16,17] and on the angular distribution of above threshold ionization electrons [18]. Only recently, standing light waves generated by intense short-pulse lasers have been applied to modify either the optical properties of a dense gas [19,20] or to characterize a beam of electrons of fs duration by electron beam diffraction [21].

In this Letter we report impulsive acceleration of neutral He atoms in an intense standing light wave of a few tens of fs duration with intensities well in the strong-field tunneling regime [22]. Observation of strong-field KD scattered atoms becomes possible in a linearly polarized laser field through the process of frustrated tunneling ionization (FTI) [23,24] as will be explained later on in more detail. Specific polarization of the two counterpropagating laser beams that form the standing wave allows for the investigation of strong-field KD scattering of neutral atoms with almost no background.

We generate a standing light wave with two counterpropagating elliptically polarized laser pulses traveling along the z axis, either corotating or counterrotating indicated by the $(+)$ or $(-)$ sign, respectively. Neglecting the laser pulse envelope for the time being we can write the fields traveling from the left and the right side $\vec{E}_l = E_0[\hat{e}_x\cos(\omega t - kz) + \hat{e}_y\epsilon\sin(\omega t - kz)]$ and $\vec{E}_r = E_0[\hat{e}_x\cos(\omega t + kz) \pm \hat{e}_y\epsilon\sin(\omega t + kz)]$, respectively. E_0 is the field strength, ω is the angular laser frequency, ϵ is the ellipticity, and the $\pm$ sign determines the helicity. All equations are given in atomic units unless stated otherwise. Adding the fields, we obtain

$$\vec{E}_{(+)} = 2E_0\cos(kz)[\hat{e}_x\cos(\omega t) + \hat{e}_y\epsilon\sin(\omega t)] \quad (1)$$

$$\vec{E}_{(-)} = 2E_0\cos(\omega t)[\hat{e}_x\cos(kz) - \hat{e}_y\epsilon\sin(kz)]. \quad (2)$$

For $\epsilon = 1$, i.e., for circularly polarized fields, the first combined field, $(+)$, is circularly polarized with an amplitude that varies spatially with $\cos(kz)$ and thus gives rise to a spatially modulated intensity along the z axis proportional to $\cos^2(kz)$. Although a standing wave is produced, strong field excitation of atoms is inhibited due to the circular polarization of the combined beam $\vec{E}_{(+)}$ [23]. In the second case $(-)$ of counterrotating circularly polarized fields, the resulting field has linear polarization which rotates with constant field amplitude periodically along the z axis.

The intensity is thus constant along the z axis without exhibiting an intensity gradient. However, for elliptically polarized laser pulses with $0 < \epsilon < 1$ the situation for the $(-)$ case differs substantially. We calculate the cycle averaged intensity for $\vec{E}_{(-)}$, Eq. (2),

$$\bar{I}(z) = \vec{\bar{E}}^2_{(-)} = E_0^2[(1+\epsilon^2) + (1-\epsilon^2)\cos(2kz)]. \quad (3)$$

Equation (3) describes a linearly polarized standing wave with a reduced visibility $v = (\bar{I}_{\max} - \bar{I}_{\min})/(\bar{I}_{\max} + \bar{I}_{\min}) = (1-\epsilon^2)/(1+\epsilon^2)$ that depends on the ellipticity of the individual fields. Most important to note is that the intensity gradient can be tuned with the help of the ellipticity of the individual beams. Finally, we multiply Eq. (3) with the time envelope of the laser pulses $f(t) = \exp(-t^2/\tau^2)$, where τ is the laser pulse duration, to obtain in a good approximation the slowly time varying cycle averaged intensity $I(z,t) = \bar{I}(z)f(t)$ of the standing light wave.

In Fig. 1(a) we show the experimental setup. By means of a beam splitter, laser pulses from a Ti:sapphire laser (1 kHz repetition rate, pulse duration 55 fs, pulse energy up to 2 mJ) are split into two pathways. The beams are then steered into a vacuum chamber from opposite sides, where they overlap in time and space to form the standing light wave. In order to assure the correct time overlap of the laser pulses the path length of one arm can be adjusted. Each laser beam, initially linearly polarized, passes through a quarter wave plate oriented at a suitable angle to adjust ellipticity ($0 < \epsilon < 0.9$) and helicity. We note that we are not able to provide perfectly circularly polarized light ($\epsilon = 1$) due to imperfections of our polarization beam splitter. Each of the two beams is then moderately focused by a lens down to a beam waist w_0 of 33 μm and 38 μm, respectively, into a well-collimated thermal atomic beam of He atoms, where atoms are excited and accelerated. The mean time of flight of excited He* atoms toward the detector is 220 μs. They can be detected by a standard position sensitive multichannel plate (MCP) detector (see, e.g., Ref. [25]), if they are still in an excited state when they hit the detector. This is likely since a large fraction of initially excited Rydberg states decay to a long-lived metastable state.

The interaction volume of the standing wave with the He beam is cylindrically shaped with a diameter of $2w_0 \cong 70$ μm and a length of about 20 μm, which is given by the short time overlap of the two counterpropagating pulses. Consequently, it is solely the standing light wave that initiates both the excitation of He atoms and the acceleration process. Each individual elliptically polarized laser beam is unable to leave He in excited states [23], so that the signal is almost background free.

In Fig. 1(b) we display a raw detector image. We observe deflected excited atoms distributed in a stripe along the z axis with a length of a few centimeters and a small width. The width of the stripe is due to the radial acceleration of atoms with respect to the beam propagation in the intensity gradient of the focused laser beam [24]. The ratio of length to width of the stripe is a direct indication of how much stronger the effective intensity gradient in the standing light wave is than in the focused laser beam. We note that we do not observe any signal if we change the helicity of the individual laser beams to the $(+)$ case as expected and also, we do not observe any signal from each individual laser beam alone. Additionally, we measured final velocity distributions for three different gases (He, Ne, and Ar)

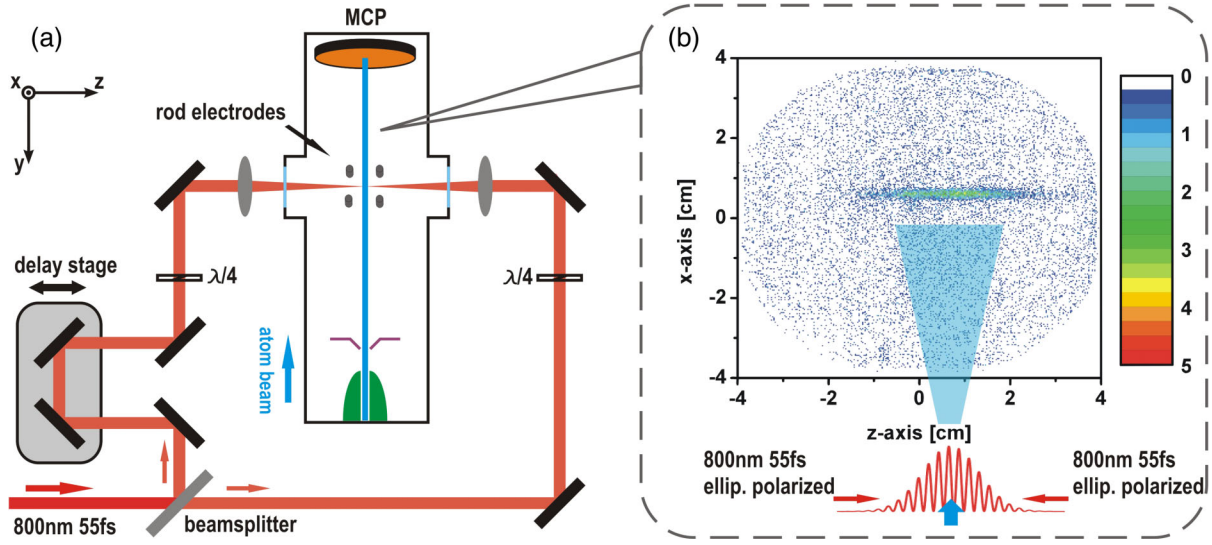

FIG. 1 (color online). (a) Experimental setup (for explanation see text). $\lambda/4$ and MCP denote quarter wave plates and multichannel plate, respectively. In (b) we display a detailed sketch of the time integrated intensity of the standing wave together with a raw detector image of the deflected He* atoms along the z axis. The number of excited He atoms impinging on the detector is color coded. The rod electrodes remove charges from strong-field ionization.

and find that the width of the distributions scales with the mass of the atom; see the Supplemental Material [26].

We performed systematic measurements by increasing the laser intensity of the standing wave while keeping the ellipticity fixed at $\varepsilon \approx 0.85$; see Fig. 2(a). In Fig. 2(b) we show results where we fixed the intensity of the standing wave at $I = 6.3 \times 10^{14}$ W cm^{-2} and adjusted the ellipticity to $\epsilon = 0.85$ and $\epsilon = 0.6$. To compare with theory we use the measured position and the time of flight to calculate the final velocity in the z direction. Inspecting the data in Fig. 2(a), we find that the overall signal increases with increasing laser intensity, but the final velocity does not. Obviously, the maximum momentum imparted on the atoms has an upper bound, either given by the fact that the atom ionizes in the strong gradient field or, that a recapture of the electron in the strong gradient field is inhibited in the first place. On the other hand, the data in Fig. 2(b) show that for $\epsilon = 0.6$ the maximum velocity is twice as high as in the case of larger ellipticity. This indicates that the maximum gradient force the atom can bear before it ionizes depends on the ellipticity and thus might be dynamically altered due to the modified interaction of the quasibound electron with the laser field.

In order to analyze our data quantitatively we recall the interpretation of excitation and acceleration of atoms [23,24]

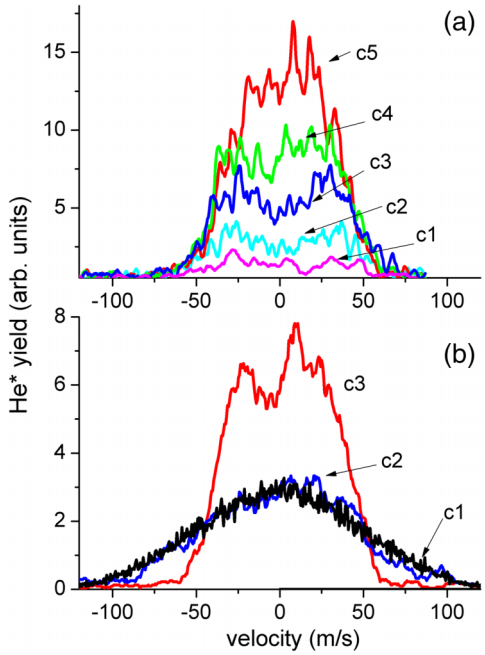

FIG. 2 (color online). Final velocity distribution of deflected He* atoms. (a) As a function of intensity I: c1: 2.5×10^{14}W cm^{-2}, c2: 3.4×10^{14} W cm^{-2}, c3: 4.2×10^{14} W cm^{-2}, c4: 5.1×10^{14} W cm^{-2}, and c5: 6.3×10^{14} W cm^{-2}. The ellipticity is fixed at $\epsilon = 0.85$. (b) as a function of ellipticity. Experimental curves, c2: $\epsilon = 0.6$ and c3: $\epsilon = 0.85$. Theoretical curve c1: $\epsilon = 0.6$. The intensity is fixed at $I = 6.3 \times 10^{14}$ W cm^{-2}. The experimental curves in (a) and (b) are smoothed. Visible structures on a small velocity scale are likely due to statistical effects.

within the tunneling picture [1,22] and simple man's model of strong-field physics [27]. An electron tunnels through the finite barrier temporarily established by the Coulomb potential and the (oscillating) laser field. Particularly those electrons that tunnel slightly before a field cycle maximum do not gain enough drift energy to escape the Coulomb potential after the laser pulse has turned off. This frustrated tunneling ionization has been found to be an important exit channel that leads to excited states [23]. During the field pulse the electron is quasifree and feels the ponderomotive force F_p, which is given for a free charged particle by the gradient of the ponderomotive potential $U_p = (q^2/2M\omega^2)\bar{I}(z)$

$$F_p = -\frac{\partial U_p}{\partial z} = -\frac{1}{2\omega^2}(q^2/M)\frac{\partial \bar{I}(z)}{\partial z}. \tag{4}$$

q is the charge and M the mass of the charged particle. Since the electron finds itself in a bound excited state after the laser pulse has terminated, the ponderomotive force accelerates the whole atom with $a_{\mathrm{cms}}(t) = (F_p/M_{\mathrm{He}})f(t)$, where M_{He} is the mass of the He atom and the subscript cms denotes the center of mass of the system. The acceleration varies with the laser pulse envelope $f(t)$, but only sets in at the instant of time t_0, when the tunneling takes place. The atomic motion is negligible on the time scale of the laser pulse [24], which gives rise to an impulsive acceleration.

In order to describe the observed velocity distribution of atoms we assume that the atoms have an effective polarizability $\alpha = 1/2\omega^2$ corresponding in good approximation to a quasifree oscillating electron in the field of an ion. The atoms are initially located in the vicinity of the field maximum at $z = 0$ between the two adjacent field minima at $z = \pm\pi/4k$. We assume the standing wave to be built up in time following $f(t)$. The number of atoms at each position is proportional to the excitation probability. This is roughly proportional to the tunneling rate of ionization, which depends on the field strength $E = I(z,t)^{1/2}$ in the standing wave. Using $F_p = -(\epsilon^2 - 1)(E_0^2/\omega^2)k\sin(2kz)$ [see Eq. (4)], the final velocity of a He atom is given by $v_f = \int_{t_0}^{\infty} a_{\mathrm{cms}}(t)dt = (F_p/M_{\mathrm{He}})\int_{t_0}^{\infty} f(t)dt$, where $S = \int_{t_0}^{\infty} f(t)dt$ can be considered an effective time of acceleration. The instant of tunneling t_0 at each z position is distributed according to the tunneling probability of the electron during the pulse. This results in a distribution of the effective acceleration time. For the calculation, we take the values for the ellipticity ϵ and for the intensities of the laser beams from the experiment. Finally, to account for the striking fact that above a certain laser intensity the final maximum velocity does not increase, we assume atoms to be ionized or not excited, if they experience a ponderomotive force that is larger than a limit set by hand, and discard them from the calculation. We remark that a full Monte Carlo trajectory calculation using the Lorentz equations for the electron and the ion including their

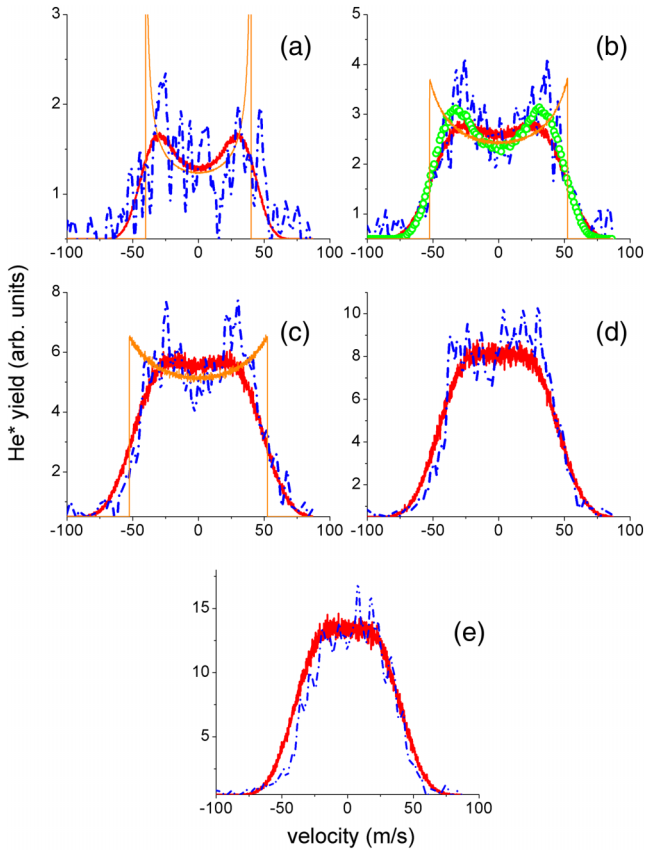

FIG. 3 (color online). Comparison of measured final velocity distributions with theoretical simulations. Blue dash-dotted curves in (a)–(e): same experimental velocity distributions as shown in Fig. 2(a), curves c1–c5, respectively. Red solid curves: Fit of the theoretical simulations to the experimental velocity distributions. Thin orange curves: Velocity distribution for fixed effective time of acceleration $S = 0.5\ \pi\tau$. Green open dots in (b): same as solid red curve, but with fit parameter $\epsilon = 0.9$.

coupling through the Coulomb force should be able to predict this limit.

The simple model calculation results in theoretical curves, which are in good agreement with the experimental data; see solid red curves in Fig. 3. The overall yield, which has been treated as a free parameter in each spectrum [Figs. 3(a)–3(e)], follows in good agreement the increasing total yield of atoms calculated by the Ammosov-Delone-Krainov (ADK) tunneling formula [28]. The relative numbers for the overall yield given in Fig. 3 are the same as in Fig. 2. $\epsilon = 0.85$ has been kept fixed for all spectra. We note, however, that treating ϵ also as an individual fit parameter in each spectrum a better agreement for individual spectra can be achieved as shown in Fig. 3(b), green curve, where we use $\epsilon = 0.9$ instead of $\epsilon = 0.85$. The velocity distribution for lower ellipticity $\epsilon = 0.6$, shown in Fig. 2(b), curve c2, reveals a maximum final velocity almost twice as high as before. Although a higher final velocity can be expected on the basis of Eqs. (3) and (4), obviously the limit of the ponderomotive force used before is not independent of ellipticity. Consequently, to model the data we have to take into account a substantially higher limit; see Fig. 2(b), curve c1.

To elucidate the ellipticity dependence, we mention that the limit of the ponderomotive force used to explain the data for $\epsilon = 0.85$, corresponds to a field strength that would ionize atoms with an effective quantum number $\nu = 4.6$. Sample classical Monte Carlo calculations for the FTI process in a standing light wave, however, show that a substantial number of atoms are left in Rydberg states with higher n quantum numbers. This indicates that the gradient force does not necessarily lead to field ionization, as one would expect from its equivalent field strength [29]. Rather it can be seen as an integral part of the dynamical process. Inclusion of the gradient force might lead as well to bound trajectories, which would not be present if the ponderomotive force were absent. In that sense, more elaborate calculations are needed to determine the limit of the ponderomotive force *ab initio*.

Finally, to get a complementary picture we treat the KD scattering in a very simplified way quantum mechanically as outlined in the Supplemental Material [26]. The results are very similar to the classical calculations. The momentum imparted on the atom in the best case corresponds to more than 400 two-photon absorptions within a 55 fs pulse duration yielding a scattering rate $\Gamma > 10^{16}\ \mathrm{s}^{-1}$.

In conclusion, we report extreme longitudinal acceleration of He atoms located in an intense short-pulse standing wave. Besides the absorption of energy corresponding to roughly 15 photons from the standing light wave we also measure the strong momentum transfer equivalent to more than 800 photon momenta during the short laser pulse. The Kapitza-Dirac scattering of neutral He atoms takes place with an unprecedented scattering rate exceeding $10^{16}\ \mathrm{s}^{-1}$. The investigation opens up new perspectives in strong-field physics by focusing on the importance of the magnetic field and on field gradients. Particularly, the existence of spatially separated pure electric and pure magnetic fields might allow for probing matter with intense magnetic fields at optical oscillation frequencies unperturbed by electric fields. Furthermore, the possibility to vary the polarization properties on an atomic scale might allow us to investigate chirality of molecules in the strong-field domain (superchiral light) [30]. Finally, we expect our experimental work to stimulate strong-field quantum mechanical calculations beyond the dipole approximation.

We acknowledge fruitful discussions with W. Becker and A. Saenz.

*eichmann@mbi-berlin.de

[1] P. B. Corkum, Phys. Rev. Lett. **71**, 1994 (1993).
[2] T. Brabec and F. Krausz, Rev. Mod. Phys. **72**, 545 (2000).
[3] P. L. Kapitza and P. A. M. Dirac, Math. Proc. Cambridge Philos. Soc. **29**, 297 (1933).

[4] S. Altshuler, L. M. Frantz, and R. Braunstein, Phys. Rev. Lett. **17**, 231 (1966).
[5] P. L. Gould, G. A. Ruff, and D. E. Pritchard, Phys. Rev. Lett. **56**, 827 (1986).
[6] C. Salomon, J. Dalibard, A. Aspect, H. Metcalf, and C. Cohen-Tannoudji, Phys. Rev. Lett. **59**, 1659 (1987).
[7] Y. B. Ovchinnikov, J. H. Müller, M. R. Doery, E. J. D. Vredenbregt, K. Helmerson, S. L. Rolston, and W. D. Phillips, Phys. Rev. Lett. **83**, 284 (1999).
[8] C. Maher-McWilliams, P. Douglas, and P. F. Barker, Nat. Photonics **6**, 386 (2012).
[9] D.-S. Guo and G. W. F. Drake, Phys. Rev. A **45**, 6622 (1992).
[10] X. Li, J. Zhang, Z. Xu, P. Fu, D.-S. Guo, and R. R. Freeman, Phys. Rev. Lett. **92**, 233603 (2004).
[11] M. A. Efremov and M. V. Fedorov, J. Phys. B **33**, 4535 (2000).
[12] O. Smirnova, D. L. Freimund, H. Batelaan, and M. Ivanov, Phys. Rev. Lett. **92**, 223601 (2004).
[13] A. E. Kaplan and A. L. Pokrovsky, Phys. Rev. Lett. **95**, 053601 (2005).
[14] P. W. Smorenburg, J. H. M. Kanters, A. Lassise, G. J. H. Brussaard, L. P. J. Kamp, and O. J. Luiten, Phys. Rev. A **83**, 063810 (2011).
[15] S. Ahrens, H. Bauke, C. H. Keitel, and C. Müller, Phys. Rev. Lett. **109**, 043601 (2012).
[16] D. L. Freimund, K. Aflatooni, and H. Batelaan, Nature (London) **413**, 142 (2001).
[17] H. Batelaan, Rev. Mod. Phys. **79**, 929 (2007).
[18] P. H. Bucksbaum, D. W. Schumacher, and M. Bashkansky, Phys. Rev. Lett. **61**, 1182 (1988).
[19] J. P. Farrell, L. S. Spector, M. B. Gaarde, B. K. McFarland, P. H. Bucksbaum, and M. Gühr, Opt. Lett. **35**, 2028 (2010).
[20] L. Shi, W. Li, Y. Wang, X. Lu, L. Ding, and H. Zeng, Phys. Rev. Lett. **107**, 095004 (2011).
[21] C. T. Hebeisen, G. Sciaini, M. Harb, R. Ernstorfer, T. Dartigalongue, S. G. Kruglik, and R. J. D. Miller, Opt. Express **16**, 3334 (2008).
[22] L. V. Keldysh, Sov. Phys. JETP **20**, 1307 (1965).
[23] T. Nubbemeyer, K. Gorling, A. Saenz, U. Eichmann, and W. Sandner, Phys. Rev. Lett. **101**, 233001 (2008).
[24] U. Eichmann, T. Nubbemeyer, H. Rottke, and W. Sandner, Nature (London) **461**, 1261 (2009).
[25] U. Eichmann, A. Saenz, S. Eilzer, T. Nubbemeyer, and W. Sandner, Phys. Rev. Lett. **110**, 203002 (2013).
[26] See Supplemental Material at http://link.aps.org/supplemental/10.1103/PhysRevLett.112.113001 for details on the quantum mechanical description of the process and on additional data for Ne and Ar atoms.
[27] H. B. van Linden van den Heuvell and H. G. Muller, in *Multiphoton Processes*, edited by S. J. Smith and P. L. Knight (Cambridge University Press, Cambridge, England, 1988).
[28] M. V. Ammosov, N. B. Delone, and V. P. Krainov, Sov. Phys. JETP **64**, 1191 (1986).
[29] E. Wells, I. Ben-Itzhak, and R. R. Jones, Phys. Rev. Lett. **93**, 023001 (2004).
[30] Y. Tang and A. E. Cohen, Science **332**, 333 (2011).